Forward-viewing resonant fiber-optic scanning endoscope of appropriate scanning speed for 3D OCT imaging

Li Huo, Jiefeng Xi, Yicong Wu, and Xingde Li*

Department of Biomedical Engineering, Johns Hopkins University, Baltimore, MD, 21205 USA
** xingde@jhu.edu*

Abstract: A forward-viewing resonant fiber-optic endoscope of a scanning speed appropriate for a high-speed Fourier-domain optical coherence tomography (FD-OCT) system was developed to enable real-time, three-dimensional endoscopic OCT imaging. A new method was explored to conveniently tune the scanning frequency of a resonant fiber-optic scanner, by properly selecting the fiber-optic cantilever length, partially changing the mechanical property of the cantilever, and adding a weight to the cantilever tip. Systematic analyses indicated the resonant scanning frequency can be tuned over two orders of magnitude spanning from ~10Hz to ~kHz. Such a flexible scanning frequency range makes it possible to set an appropriate scanning speed of the endoscope to match the different A-scan rates of a variety of FD-OCT systems. A 2.4-mm diameter, 62.5-Hz scanning endoscope appropriate to work with a 40-kHz swept-source OCT (SS-OCT) system was developed and demonstrated for 3D OCT imaging of biological tissues.

OCIS codes: (110.4500) Optical coherence tomography; (120.5800) Scanner; (170.3880) Medical and biological imaging

References and links

1. M. A. Choma, M. V. Sarunic, C. H. Yang, and J. A. Izatt, "Sensitivity advantage of swept source and Fourier domain optical coherence tomography," Opt. Express **11**(18), 2183–2189 (2003).
2. J. F. de Boer, B. Cense, B. H. Park, M. C. Pierce, G. J. Tearney, and B. E. Bouma, "Improved signal-to-noise ratio in spectral-domain compared with time-domain optical coherence tomography," Opt. Lett. **28**(21), 2067–2069 (2003).
3. R. Leitgeb, C. K. Hitzenberger, and A. F. Fercher, "Performance of fourier domain vs. time domain optical coherence tomography," Opt. Express **11**(8), 889–894 (2003).
4. A. F. Fercher, C. K. Hitzenberger, G. Kamp, and S. Y. Elzaiat, "Measurement of Intraocular Distances by Backscattering Spectral Interferometry," Opt. Commun. **117**(1-2), 43–48 (1995).
5. B. Potsaid, I. Gorczynska, V. J. Srinivasan, Y. L. Chen, J. Jiang, A. Cable, and J. G. Fujimoto, "Ultrahigh speed spectral / Fourier domain OCT ophthalmic imaging at 70,000 to 312,500 axial scans per second," Opt. Express **16**(19), 15149–15169 (2008).
6. S. R. Chinn, E. A. Swanson, and J. G. Fujimoto, "Optical coherence tomography using a frequency-tunable optical source," Opt. Lett. **22**(5), 340–342 (1997).
7. R. Huber, D. C. Adler, and J. G. Fujimoto, "Buffered Fourier domain mode locking: Unidirectional swept laser sources for optical coherence tomography imaging at 370,000 lines/s," Opt. Lett. **31**(20), 2975–2977 (2006).
8. M. Kuznetsov, W. Atia, B. Johnson, and D. Flanders, "Compact Ultrafast Reflective Fabry-Perot Tunable Lasers For OCT Imaging Applications," Proc. SPIE **7554**, 75541F (2010).
9. J. F. Xi, L. Huo, Y. C. Wu, M. J. Cobb, J. H. Hwang, and X. D. Li, "High-resolution OCT balloon imaging catheter with astigmatism correction," Opt. Lett. **34**(13), 1943–1945 (2009).
10. X. D. Li, C. Chudoba, T. Ko, C. Pitris, and J. G. Fujimoto, "Imaging needle for optical coherence tomography," Opt. Lett. **25**(20), 1520–1522 (2000).
11. X. M. Liu, M. J. Cobb, Y. C. Chen, M. B. Kimmey, and X. D. Li, "Rapid-scanning forward-imaging miniature endoscope for real-time optical coherence tomography," Opt. Lett. **29**(15), 1763–1765 (2004).
12. Y. L. Wang, M. Bachman, G. P. Li, S. G. Guo, B. J. F. Wong, and Z. P. Chen, "Low-voltage polymer-based scanning cantilever for in vivo optical coherence tomography," Opt. Lett. **30**(1), 53–55 (2005).
13. Y. T. Pan, H. K. Xie, and G. K. Fedder, "Endoscopic optical coherence tomography based on a microelectromechanical mirror," Opt. Lett. **26**(24), 1966–1968 (2001).

#128404 - $15.00 USD Received 13 May 2010; revised 6 Jun 2010; accepted 14 Jun 2010; published 21 Jun 2010

14. J. M. Zara, S. Yazdanfar, K. D. Rao, J. A. Izatt, and S. W. Smith, "Electrostatic micromachine scanning mirror for optical coherence tomography," Opt. Lett. **28**(8), 628–630 (2003).
15. J. G. Wu, M. Conry, C. H. Gu, F. Wang, Z. Yaqoob, and C. H. Yang, "Paired-angle-rotation scanning optical coherence tomography forward-imaging probe," Opt. Lett. **31**(9), 1265–1267 (2006).
16. M. T. Myaing, D. J. MacDonald, and X. D. Li, "Fiber-optic scanning two-photon fluorescence endoscope," Opt. Lett. **31**(8), 1076–1078 (2006).
17. L. E. Kinsler, A. R. Frey, A. B. Coppens, and J. V. Sanders, in *Fundamentals of Acoustics*(Wiley, New York, 1982).
18. D. L. Wang, B. V. Hunter, M. J. Cobb, and X. D. Li, "Super-achromatic rapid scanning microendoscope for ultrahigh-resolution OCT imaging," IEEE J. Sel. Top. Quantum Electron. **13**(6), 1596–1601 (2007).

1. Introduction

Recent development in the Fourier-domain optical coherence tomography (FD-OCT) technology [1–3] has significantly improved the imaging speed. It has been reported that several hundreds of kHz A-scan rate can be achieved with both the spectral-domain OCT (OCT) [4], enabled by high-speed CMOS line camera [5], and the swept-source OCT (SS-OCT) [6], enabled by fast Fourier-domain mode-locked laser (FDML) [7] or short-cavity swept laser [8]. With the increase in imaging speed, real-time, three-dimensional (3D) OCT imaging becomes possible.

At the same time, efforts have been devoted to developing OCT endoscopes to enable imaging of internal organs. There are two categories of endoscopes for different endoscopic OCT applications. One has a side-viewing design such as a balloon catheter [9] and an OCT imaging needle [10]. In this type of endoscopes, distal end circumferential beam scanning is achieved by rotating the entire probe by a rotary joint at the proximal end with an upper speed limit of ~50-100 rounds/second. The other type is the forward-viewing probe which allows for imaging tissues in front of the probe and it is easy to position the probe over target area by gentle contact with the tissue. There are several methods available to make a forward-viewing endoscope, e.g., by using a tubular PZT actuator [11] or deformable memory polymer [12] to swing the imaging fiber cantilever, by using a MEMS scanner [13,14] or by using paired-angle-rotation lens to scan the optical beam [15]. The scanning device in a forward-viewing endoscope is usually placed at the distal end, thus there is strict requirement for a small footprint. Among the forward-viewing endoscopes reported so far, the paired-angle-rotation lens makes the smallest diameter (1.65 mm). However, this configuration requires precision alignment throughout continuous rotation, and 3D imaging speed can be limited by the rotary joint. An MEMS mirror has a fast scan frequency; the challenge with such a scanner is its fairly large size (e.g., 5-mm probe diameter in ref [13]. due to its relatively large package footprint and the requirement of folding the beam path). The resonant fiber-optic scanner is an attractive alternative for forward-viewing applications by providing an excellent combination of small size and fast scanning speed. The tubular PZT actuator can be made very thin (e.g., 1.0-1.8 mm) and it does not require any beam folding for forward-viewing. At the same time, the scanning speed can be easily tuned over a large range. The resonant fiber-optic scanner employees a spiral-scanning pattern over a circular field of view instead of the conventional raster-scanning pattern. The main disadvantage of such pattern is the non-uniformity of sampling density throughout the field of view, i.e., the center part has a much higher sampling density than the peripheral part. In practice, the sampling density of the outermost part should be sufficiently high to satisfy the Nyquist sampling limit regarding to the lateral resolution.

Previously, we have demonstrated a forward-imaging endoscope based on a resonant fiber-optic scanner with a rapid scanning speed in the range of ~kHz for a time-domain OCT (TD-OCT) system [16]. With the development of high-speed FD-OCT technologies, the overall time needed to collect the 3D volumetric data can be significantly reduced. However, FD-OCT acquires all the depth information at a given lateral position with a single A-scan before the beam is moved to the next lateral position (axial priority sequence). The dwell time of the scanning beam on a lateral point is significantly different with that of the TD-OCT. Endoscope with an appropriate scanning speed is thus required to match the speed of an FD-OCT system. For an FD-OCT system of a 50-kHz A-scan rate, if we assume each frame

#128404 - $15.00 USD Received 13 May 2010; revised 6 Jun 2010; accepted 14 Jun 2010; published 21 Jun 2010

consists of 500 A-scans, the scanning speed required for the endoscope is 100 Hz. Considering the A-scan rates of the reported FD-OCT systems vary between ~20-500 kHz, the corresponding scanning frequency of the resonant fiber cantilever will be in the range of 40-1,000 Hz. Therefore a convenient and generic method is needed to tune the scanning frequency throughout one or two orders of magnitude to appropriately match the various speeds of different FD-OCT systems.

In this paper, we proposed and demonstrated a method to tune the resonant frequency of a PZT-actuated resonant fiber-optic scanner with a modified structure by selecting a proper length for the fiber cantilever, partially changing the mechanical property of the cantilever, and adding additional weight on the cantilever tip. Systematic vibration mode analyses of the cantilever show that the resonant frequency can be effectively controlled over two orders of magnitude spanning from ~10Hz to ~kHz. The extended frequency tuning range provides the flexibility for the endoscope to match the different speeds of FD-OCT systems. A 2.4-mm diameter forward-viewing prototype endoscope with a 62.5-Hz resonant frequency appropriate for a 40-kHz SS-OCT system was developed and demonstrated for high-speed 3D and *en face* OCT imaging *in vivo*.

2. Working principle and theoretical design analyses

The scanning speed of the PZT-actuated resonant fiber-optic scanner depends on the mechanical resonant frequency of its fiber cantilever, and the frequency of driving signal applied to the PZT must be tuned to the resonant frequency in order to obtain a maximum scanning field. In our previous designs [11,16], the resonant frequency ω of the fiber-optic cantilever is given by Eq. (1) [17]:

$$\omega = \beta \left(\frac{E}{\rho} \right)^{\frac{1}{2}} \frac{R}{L^2}, \tag{1}$$

where β is a mode-related constant, E, ρ, R and L represent the Young's modulus, mass density, radius and length of the fiber cantilever, respectively. For a single-mode fiber (SMF such as SMF-28) with a diameter 125 μm, the resonant frequency is ~1 kHz for a cantilever length L = 10 mm. To reduce the resonant frequency to ~100 Hz, several solutions can be considered. The first method is to thin the radius of the fiber cantilever by 10 times through chemical etching. However, this approach might be problematic due to the resulted mechanical fragility, potential leakage of guided light and difficulty in controlling the etching uniformity. The second method is to use a longer cantilever, i.e. ~33-mm long for reducing the resonant frequency down to ~100 Hz. The endoscope made of such a long cantilever would have a long rigid length after packaging and become difficult to pass through the Y-shape entry port of a standard gastroscope. The third approach is to put additional weight to the cantilever and change its mechanical property, which is equivalent to changing the ratio of E and ρ. In this study, we first investigate how the resonance frequency can be changed with the combination of different cantilever length and additional weight added to the cantilever.

The modified structure of a resonant fiber-optic scanner is schematically shown in Fig. 1. The distal portion of the SMF cantilever is covered with a stainless hypodermic tube of an ultrathin wall, which adds an additional weight to the cantilever and partially changes its mechanical property. The uncovered end of the SMF is fixed (i.e., to the PZT actuator) and the end covered by the hypodermic tube is kept free. This mechanical system can be modeled as a two-sectional stepped beam with one clamped end and one free end. Each section has its specific diameter, mass density and elasticity. There are innumerous vibration modes in this system. In this research, we are only interested in the fundamental transversal vibration mode which is used in the experiment.

#128404 - $15.00 USD Received 13 May 2010; revised 6 Jun 2010; accepted 14 Jun 2010; published 21 Jun 2010

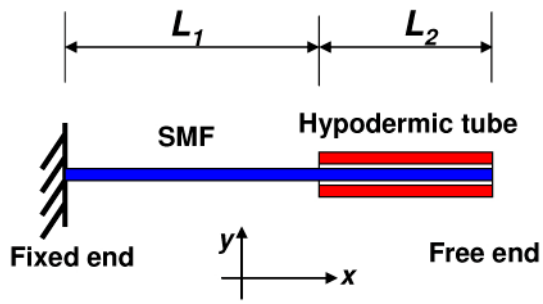

Fig. 1. The schematic of the hybrid fiber cantilever with a hypodermic metal tube covering the free end of the cantilever.

The general transversal vibration solution of each section of the beam can be written as Eq. (2) [17]:

$$y_i(x) = C_i^1 \sin K_i x + C_i^2 \sinh K_i x + C_i^3 \cos K_i x + C_i^4 \cosh K_i x, \tag{2}$$

where y_i is the vertical displacement of the ith section (i=1,2) of the cantilever and

$$K_i^2 = \left(\frac{\rho A}{EI_i}\right)^{\frac{1}{2}} \omega. \tag{3}$$

Here in Eq. (3) A and I represent the cross-sectional area and the second moment of inertia of the ith section, respectively. C_i^j (i=1,2; j=1,2,3,4) are constants to be determined. By applying proper boundary conditions and connective conditions of continuity in displacements, displacement slopes, moments and shear forces on different sections, one can obtain the following equation if a nontrivial solution of C_i^j in Eq. (2) exists:

$$\begin{vmatrix} \sin q_1 - \sinh q_1 & \cos q_1 - \cosh q_1 & -\sin q_2 - \sinh q_2 & -\cos q_2 - \cosh q_2 \\ \cos q_1 - \cosh q_1 & -\sin q_1 - \sinh q_1 & \frac{K_2}{K_1}(\cos q_2 + \cosh q_2) & \frac{K_2}{K_1}(\sinh q_2 - \sin q_2) \\ -\sin q_1 - \sinh q_1 & -\cos q_1 - \cosh q_1 & (\frac{K_2}{K_1})^2 \frac{I_2}{I_1}(\sin q_2 - \sinh q_2) & (\frac{K_2}{K_1})^2 \frac{I_2}{I_1}(\cos q_2 - \cosh q_2) \\ -\cos q_1 - \cosh q_1 & \sin q_1 - \sinh q_1 & (\frac{K_2}{K_1})^3 \frac{I_2}{I_1}(\cosh q_2 - \cos q_2) & (\frac{K_2}{K_1})^3 \frac{I_2}{I_1}(\sin q_2 + \sinh q_2) \end{vmatrix} = 0, \tag{4}$$

where $q_i = K_i L_i$ and L_i is the length of the ith section of the cantilever.

Equation (4) is only a function of the resonant frequency ω, and it can be solved numerically. There is more than one solution with each solution representing a different resonant frequency of transversal vibration modes. The fundamental resonant frequency of interest in our study is obtained as the one with the smallest absolute value.

Figure 2 shows the contour plot of the calculated resonant frequency of the hybrid cantilever as a function of the total SMF cantilever length and the ratio of the cantilever covered by a stainless hypodermic tube. The frequency was calculated based on a 305/406-µm inner/outer diameter stainless hypodermic tube, as used in experiments, added to the distal end of a 125-µm SMF cantilever.

In the previous design, only the cantilever length L could be used to tune the resonant frequency according to Eq. (1). The available scanning frequency range is thus limited due to the concern of the cantilever length and so forth the overall rigid length of the endoscope. With the modified cantilever structure as described above, the tunable frequency range is significantly extended without significantly increasing the cantilever length. As shown in Fig. 2, for a reasonable cantilever length below 20 mm, the resonant scanning frequency can be tuned between ~1 kHz to ~60 Hz by carefully selecting the combination of the total cantilever

#128404 - $15.00 USD Received 13 May 2010; revised 6 Jun 2010; accepted 14 Jun 2010; published 21 Jun 2010

length and the metal tube length. The wide resonant frequency range provides the flexibility to match a wide range of FD-OCT systems with A-scan rates varying between ~30 kHz to ~500 kHz. Figure 2 also indicates that the slowest resonant scanning frequency can be achieved for a 20-mm fiber cantilever when ~50% of the cantilever is covered by a metal tube. In this paper, our target resonant frequency is around ~60 Hz in order to match a 40-kHz FDML-based SS-OCT system.

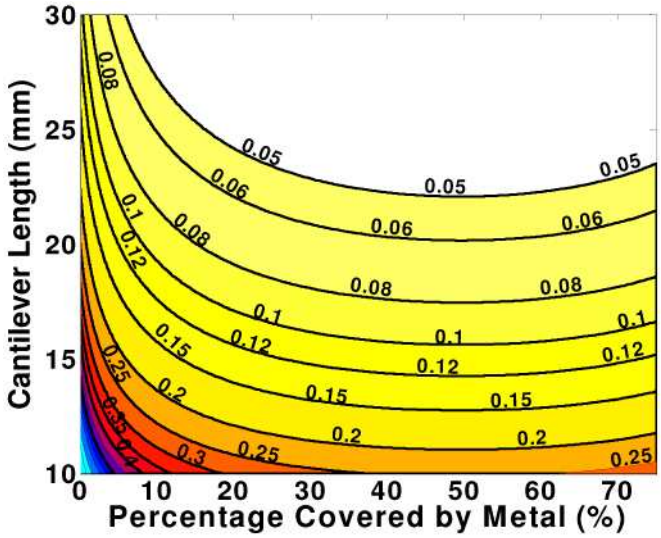

Fig. 2. Contour plot of the resonant frequency as a function of the total SMF cantilever length and the percentage of the cantilever covered by a stainless hypodermic tube. Frequency units: kHz

Due to the resonant nature of the scanning scheme, the scanning frequency is fixed once the probe is made. However, the above theoretical analysis provides a very good prediction of the probe configuration required for a given resonant frequency, which is pre-determined to match a given FD-OCT imaging speed. The resonance frequency can then be easily tuned/changed according to the design configuration during probe engineering.

3. Endoscope configuration and performance

Figure 3(A) illustrates the design schematic of the modified endoscope. It entails a tubular PZT actuator, a fiber-optic cantilever attached to the end of the PZT actuator, and a microlens to image the sweeping fiber tip to the sample. Specifically in this prototype, a 20-mm SMF cantilever was first made with a measured resonant frequency of 250 Hz. A 9-mm stainless hypodermic tube with a 305/406-µm inner/outer diameter was then glued onto the fiber cantilever tip, which resulted in a final measured resonant frequency of 62.5 Hz. Figure 3(B) shows a picture of the resonating fiber-optic cantilever. With a drive voltage of ±40V, a tip-scanning range of 2 mm was achieved. 2D *en face* scanning was performed with a spiral-scanning pattern when the X and Y electrodes were driven by two triangularly-modulated sinusoidal waves with a 90° phase difference. The beam from the fiber tip was focused by a 0.29-pitch, 1.8-mm diameter GRIN lens at a working distance of 2.45 mm. A GRIN lens, which has been widely used in OCT endoscopes, was chosen here as the focusing element simply for the proof-of-concept demonstration. It is understood that a customized micro-compound lens with reduced chromatic and spherical aberration, similar to the one we developed for 800 nm [18], can be used to improve the image quality in the future. The lateral scanning range of the cantilever tip was magnified by 1.4 times onto the tissue by the GRIN lens. The lateral resolution was measured to be 13 µm with a confocal parameter of 200 µm (for a center source wavelength at 1310 nm). The PZT actuator, the fiber cantilever and the GRIN lens were finally encased into a protective detachable hypodermic tube of a 2.4-mm

#128404 - $15.00 USD Received 13 May 2010; revised 6 Jun 2010; accepted 14 Jun 2010; published 21 Jun 2010

outer diameter. Figure 3(C) shows a photo of the finished resonant fiber-optic scanning OCT endoscope.

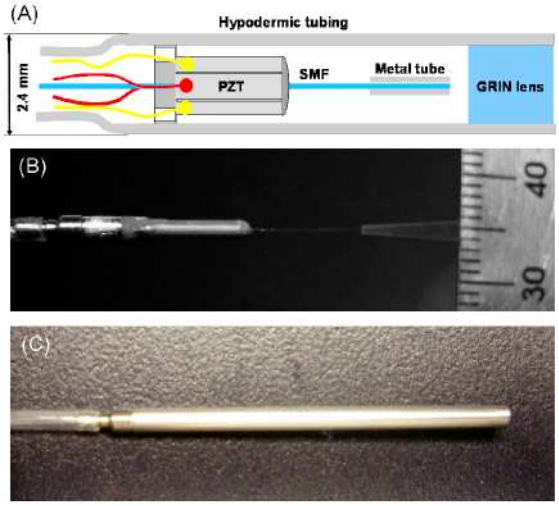

Fig. 3. (A) Schematic of the forward-viewing endoscope of an appropriate scanning frequency for a 40-kHz SS-OCT system. SMF: single-mode fiber, MT: metal tube. (B) Photo of a resonating hybrid fiber-optic cantilever at a frequency of 62.5 Hz. (C) Photo of the assembled forward-viewing endoscope of a 2.4-mm diameter.

The frequency response of the prototyped hybrid cantilever, i.e. scan amplitude versus driving frequency, was also measured around the resonance frequency of 62.5 Hz. The Q factor of the resonance peak was ~78 with a 3-dB bandwidth of ~0.8 Hz. By fitting the measured data to the frequency response of a damped harmonic oscillator, the damping time was found to be 0.56 s.

4. 3D OCT imaging of biological tissues with the resonant fiber-optic scanning endoscope

Real-time 3D OCT imaging with the forward-viewing endoscope was experimentally demonstrated by using a SS-OCT system as shown in Fig. 4. The light source used in the experiment was a 40-kHz FDML swept source, which had a 3-dB spectral bandwidth of ~110 nm and a full bandwidth of 150 nm with a center wavelength at 1310 nm. The average output power was 35 mW. The measured OCT axial resolution was 9.7 μm in air and the detection sensitivity was ~110 dB at an incident power of ~20 mW on the sample. 5% of the optical power from the FDML was delivered to a Mach-Zenhder interferometer (MZI) for calibration. The optical path length difference between the two arms of the calibration MZI was set as 5 mm, corresponding to an imaging depth of 2.5 mm in air and 1.78 mm in tissue. A dual-balanced photodetector was used to detect the interference signal for calibration. The rest 95% of the source power was sent into the OCT imaging system which is also composed of an MZI and a dual-balanced detector. A neutral density filter (ND) was used in the reference arm to optimize the detection sensitivity. The same 62.5-Hz resonant fiber-optic scanning endoscope as we described and characterized in Section 3 was incorporated in the OCT sample arm and the interference signal was collected by a data acquisition card at 180 MSample/s with 16-bit resolution. OCT images were acquired, processed, displayed and stored in real time at a rate of 62.5 frame/sec with each frame consisting of 652 × 2048 pixels (circumferential × axial). For 3D data reconstruction, each frame was mapped onto a cylindrical surface and there were totally 512 concentric cylindrical surfaces in each volumetric data set. It took 8.3 s to acquire the 512 × 652 × 2048 pixels (radial × circumferential × axial) volumetric data with only one *en face* scan.

#128404 - $15.00 USD Received 13 May 2010; revised 6 Jun 2010; accepted 14 Jun 2010; published 21 Jun 2010

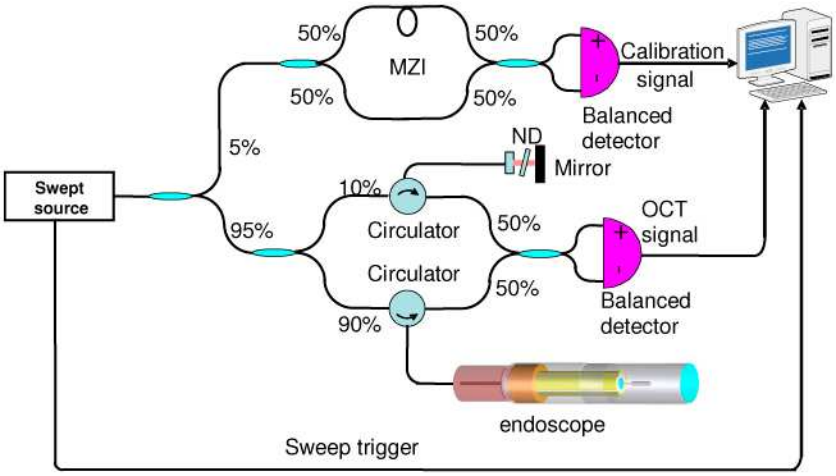

Fig. 4. Schematic of the SS-OCT system based on a 40-kHz FDML source

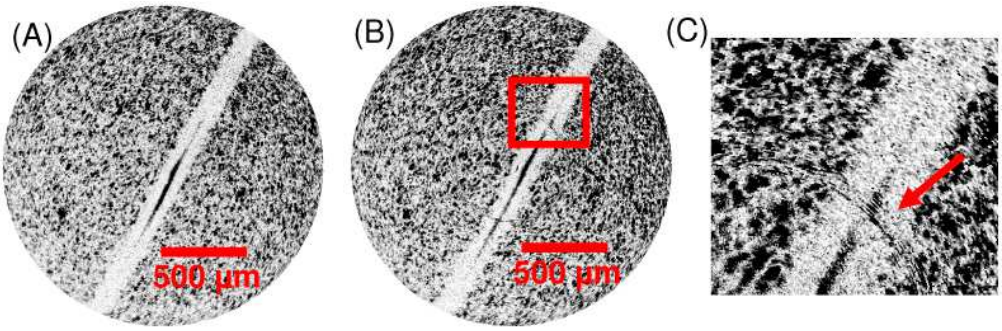

Fig. 5. *En face* images of a segment of SMF embedded in a scattering phantom. (A) The endoscope was static. The bright area shows the SMF. (B) The endoscope was tapped during imaging. The red box includes part of the disrupted area due to tapping. (C) Zoom-in view of the region indicated by the red box in (B). Motion artifact is indicated by the red arrow.

To evaluate the image quality as well as potential motion artifacts with this endoscope, a small segment of bare SMF (SMF-28) of 125-µm diameter was used as a standard sample. The SMF was embedded in a phantom made of gelatin and TiO_2 granules at 1mg/ml concentration. Figure 5(A) shows the reconstructed *en face* OCT image of the sample in which the SMF can be easily identified. The thickness of the SMF was quite uniform throughout the field of view of 2-mm diameter. To estimate potential motion artifacts, we intentionally tapped the probe during imaging, and the resulted *en face* image is shown in Fig. 5(B) which did not exhibit significant global difference compared to Fig. 5(A) (where no tapping was introduced). However, we did observe some temporary motion artifacts over a small region at a certain radial distance (as indicated by the red box in Fig. 5(B)) when the probe was tapped. Figure 5(C) shows a zoom-in view of the boxed region in Fig. 5(B). The motion artifacts were manifested as some rings with irregular pattern (indicated by the arrow). Shortly after the disruption, the continuously actuated cantilever returned to its normal scanning pattern. The duration of the disturbance was estimated to be ~0.4 s which is consistent with the previously measured damping time of ~0.56 s. This result suggested that when the endoscope was moved to a different site of the tissue, ~0.4-0.6-s stabilization time was required to avoid motion artifacts. In practice, the probe is placed on tissue surface with gentle pressure, which helps reduce motion artifacts.

#128404 - $15.00 USD Received 13 May 2010; revised 6 Jun 2010; accepted 14 Jun 2010; published 21 Jun 2010

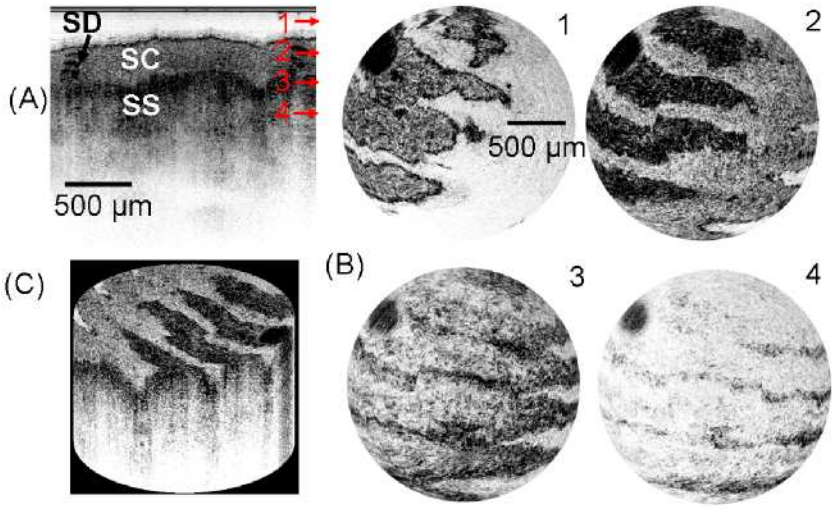

Fig. 6. *In vivo* human finger OCT images. (A) A reconstructed diametric cross-sectional image. (B) 4 reconstructed *en face* images at different depths 320-µm apart as indicated by the red arrows in Fig. 6(A). (C) A reconstructed 3D image with a cut-away view from the layer as shown in Fig. 6(B)-2. SC: stratum corneum, SD: sweat duct, SS: stratum spinosum.

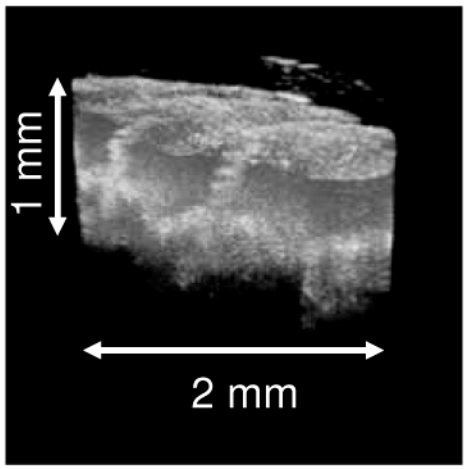

Fig. 7. Reconstructed 3D view of human finger *in vivo* captured with the endoscope. The movie shows the rotation of the sample, followed by a fly-through along the axial direction (Media 1) (3.9MB).

Different biological samples were imaged with the endoscope *in vivo*. When performing *in vivo* OCT imaging, the entire endoscope was snug fitted into a plastic protective tube and a transparent plastic wrap was used to cover the distal end of the plastic tube in order to protect the optical components inside the endoscope from contacting the tissue or biofluid. During imaging, the endoscope was gently rested on the tissue surface (through the transparent wrap) which minimized potential motion artifacts. All the samples presented below were imaged in a cylindrical volume with a diameter of 2 mm and a depth of 1.78 mm in tissue. As an example, Fig. 6 shows *in vivo* OCT images of human fingertip with a representative reconstructed diametric cross-sectional image [Fig. 6(A)], four *en face* images [Fig. 6(B)] at different tissue depths 320-µm apart, and a reconstructed 3D image with a cut-away cross-section view [Fig. 6(C)]. Figure 7 shows a movie of the reconstructed 3D view of the finger tip with a rotation of the sample followed by a fly-through in axial direction. The stratum corneum, sweat ducts, and fingerprint ridges could be clearly identified.

#128404 - $15.00 USD Received 13 May 2010; revised 6 Jun 2010; accepted 14 Jun 2010; published 21 Jun 2010

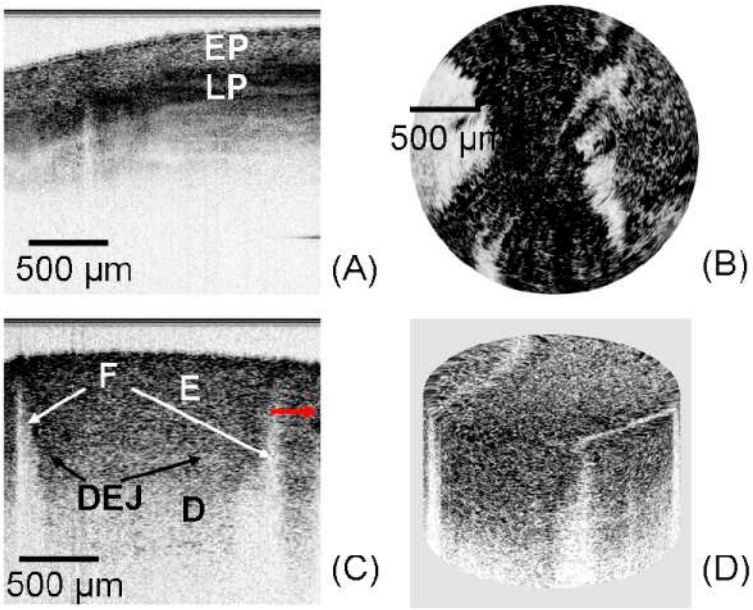

Fig. 8. OCT images of different oral cavity tissues *in vivo*. (A) A reconstructed diametric cross-sectional image of the mucosa at the lower lip. (B) Reconstructed *en face* image of the tongue. (C) A reconstructed diametric cross-sectional image of the tooth. (D) Reconstructed 3D image of the tooth with a cut-away view from the depth as indicated in Fig. 8(C). EP: epithelium, LP: lamina propria, E: facial enamel, D: dentin, DEJ: dentin-enamel junction, F: fault

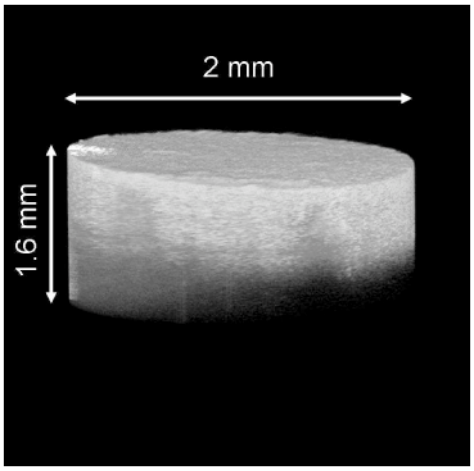

Fig. 9. Reconstructed 3D view of human canine tooth *in vivo* captured with the endoscope from the side of the tooth. The movie shows the rotation of the sample, followed by a fly-through in the axial direction (Media 2). (1.2MB)

The small footprint of the endoscope permits its access to most parts of the oral cavity, including both the soft and the hard tissues. *In vivo* 3D OCT images of the oral cavity were captured at the lower lip mucosa, tongue, and tooth as shown in Fig. 8. Figure 8(A) shows a representative reconstructed diametric cross-sectional image of the lower-lip mucosa in which layered structures of epithelium (EP) and lamina propria (LP) are clearly identified. Figure 8(B) shows a reconstructed *en face* image of the tongue where one can easily see the papilla structures. Figure 8(C) shows a diametric cross-sectional image of the canine tooth

#128404 - $15.00 USD Received 13 May 2010; revised 6 Jun 2010; accepted 14 Jun 2010; published 21 Jun 2010

where the facial enamel (E), dentin (D), and the junction (DEJ) are distinct. The faults which likely occurred during the development of the tooth are also apparent in this image. Figure 8(D) shows a reconstructed 3D image of the tooth with a cut-away view from the depth as indicated by the red arrow in Fig. 8(C). The orientation of the faults can be readily observed. Figure 9 demonstrates a movie of the reconstructed 3D view of the tooth. No severe motion artifacts were observed during the volumetric imaging process.

5. Conclusion

In summary, we developed and demonstrated a convenient method to control the resonant frequency of a PZT-actuated fiber-optic cantilever over a large range, so that an endoscope based on such a fiber-optic scanner can match the speed requirement of various SS-OCT systems for high-speed real-time 3D volumetric imaging. Systematic analyses of the scanning frequency of the modified fiber-optic cantilever show that the resonant frequency can be easily controlled between ~10Hz to ~kHz with the combination of the cantilever length and an additional mass attached on the cantilever. A prototype forward-viewing endoscope has been developed based on the modified resonant fiber-optic scanner of a 62.5 Hz scanning frequency to accommodate a 40-kHz FDML SS-OCT system. Three-dimensional volumetric data set of the tissue was obtained with only one *en face* scan. It is noted that the forward-imaging endoscope can also be easily modified to a side-viewing configuration by adding a reflector after the focusing lens for imaging the tissue in parallel with (as opposed to in front of) the endoscope.

Acknowledgements

The authors would like to acknowledge the funding support from the National Institutes of Health (NIH) (R21 CA116442, R01 CA120480 and 1R01 EB007636) and the National Science Foundation (NSF) Career Award (XDL).

#128404 - $15.00 USD Received 13 May 2010; revised 6 Jun 2010; accepted 14 Jun 2010; published 21 Jun 2010